Theory of *in situ* measurement of wave-vector-dependent dynamic susceptibility and ESR spectroscopy using the ac Josephson effect

S. E. Barnes
Department of Physics, University of Miami, Coral Gables, Florida 33124

F. Mehran
IBM, Thomas J. Watson Research Center, Yorktown Heights, New York 10598
(Received 27 December 1985)

The elementary theory of *in situ* measurements of the wave-vector-dependent dynamic susceptibility $\chi(q,\omega)$ in superconductor-insulator-superconductor (*SIS*) and superconductor—normal-metal—superconductor (*SNS*) Josephson junctions is presented in some detail. The theory for more complicated *SISN* and *SINS* junctions is also described. In addition, the theory of point-contact and superconducting quantum interference device geometries, relevant to the recent experiments of Baberschke, Bures, and Barnes is developed. Involved is a detailed application of the Maxwell and London equations along with the distributed Josephson effect. In a measurement of $\chi(q,\omega)$, the frequency ω is determined by the relation $2eV_0=\hbar\omega$ where V_0 is the voltage applied across the junction, and the wave vector q is determined by the relation $2edB_0=\hbar q$ where d is the effective width of the junction and B_0 is the magnetic field applied perpendicular to the direction of the current. The relative merits of the different types of junctions are discussed and the expected signal strengths are estimated. The limitations for the maximum measurable frequency and wave vector are also given. It seems probable that the proposed technique can be used to measure spin-wave branches from zero wave vector up to about 10% of the way to the Brillouin zone edge. The electron-spin resonance (ESR) of dilute magnetic systems can be measured as in the experiments of Baberschke, Bures, and Barnes. Estimates and experiment suggest that this method of performing ESR is better than an order of magnitude more sensitive than conventional methods. Some applications are discussed.

I. INTRODUCTION

The idea of using the ac Josephson effect to perform spectroscopic measurements is not new. Many years ago Silver and Zimmerman[1] studied the nuclear magnetic resonance (NMR) of ^{59}Co in this way. However, it was not until some time later that one of the present authors[2] suggested the appropriateness of this effect for the *in situ* detection of ESR in metals and superconductors. The *in situ* nature of the measurements avoids the well-known mismatch of Josephson junctions to microwave components and the equally bad impedance difference between such components and the metallic or superconducting sample.

A point-contact method for the fabrication of superconductor—normal-metal—superconductor (*SNS*) junctions has recently been developed by Pellison *et al.*[3] In such structures the N layer comprises a suitable sample. The first successful ESR measurements on such *SNS* junctions with samples of both Au:Er and Au:Gd have recently been reported.[4,5] It is easily possible to measure samples of Au:Gd with as little as 100 ppm of the magnetic ion Gd^{3+}. This concentration is only a few times the practical sensitivity limit of the conventional ESR instruments.

Very recently Goldman *et al.*[6] and the present authors have extended the idea to measurements of the q-dependent dynamic susceptibility $\chi(q,\omega)$ in concentrated magnets. Goldman *et al.*[6] effectively used an adaptation of the theory for the Eck modes.[7] However, it is known that the implicit assumptions of the theory which leads to Eck modes are not always justified. When these assumptions are avoided one obtains the theory for the Fiske modes.[8,9] Only in the large frequency limit do the many such Fiske modes merge into an Eck mode. In this limit the Eck mode is the envelope of the Fiske modes. Unfortunately, whatever limit one takes, the approach of Ref. 6 is invalid since it ignores the displacement current, which directly implies that both Fiske and Eck modes are absent. As Goldman *et al.*[6] state, one might justify ignoring the displacement current for frequencies much less than that of the first Fiske mode. However, as we will show in Sec. III, in this case the coupling to the susceptibility with a wave vector determined by the field is of the same order as the coupling to the lowest wave-vector susceptibility, implying the technique is nonspecific with respect to the wave vector. It is the specification of the wave vector using the magnetic field which is the principal point of the proposed experiment. It will also be shown that this problem can be avoided by using other geometries.

The basic applications of the Maxwell, London, and Josephson equations to the problem of planar superconductor-insulator-superconductor (*SIS*) and *SNS* junctions are described in some detail in Sec. II. The spectroscopic response of such junctions is calculated in Sec. III. Also dealt with in this section is the adaptation

of the theory to point contact and superconducting quantum interference device (SQUID) type of geometries. The estimation of the actual magnetic signal strengths which are expected in $\chi(q,\omega)$ or ESR measurements is given in Sec. IV. Section V contains our conclusions and a discussion of possible applications for the present technique.

II. BASIC THEORY

In this section we describe the basic theory involved in spectroscopic measurements in a standard planar Josephson junction *SMS*, where *M* stands for either an insulating (*I*) or a normal conducting (*N*) barrier separating the two superconducting (*S*) layers. As illustrated in Fig. 1, the junction is of rectangular shape with a barrier of thickness $2a$ along the x axis and length L along the z axis. Either the *M* or the *S* layers may be magnetically doped.

The problem to be considered is that of a damped strip-line resonator. The role of the ac Josephson effect is twofold: to provide the driving current for the strip line and to detect its resulting resonances. This problem has previously been analyzed[7-9] for undoped *SIS* junctions and the theory of the resulting Eck[7] or Fiske[8,9] modes is well confirmed by experiment.[7,9] The response of undoped *SNS* junctions has also been investigated both theoretically[10] and experimentally.[11] We will extend these theories to junctions doped with magnetic impurities. Since our conclusions do not agree with the recent work of Goldman *et al.*,[6] we will give sufficient detail for the reader to follow the various steps with reasonable ease.

We begin with the Maxwell equations

$$\nabla\times\mathbf{E}=-\frac{\partial\mathbf{B}}{\partial t}\,, \tag{2.1}$$

$$\nabla\times\mathbf{H}=\frac{\partial\mathbf{D}}{\partial t}+\mathbf{j}\,. \tag{2.2}$$

In general, the current density $\mathbf{j}$ is given by

$$\mathbf{j}=\mathbf{j}_N+\mathbf{j}_S+\mathbf{j}_J\,, \tag{2.3}$$

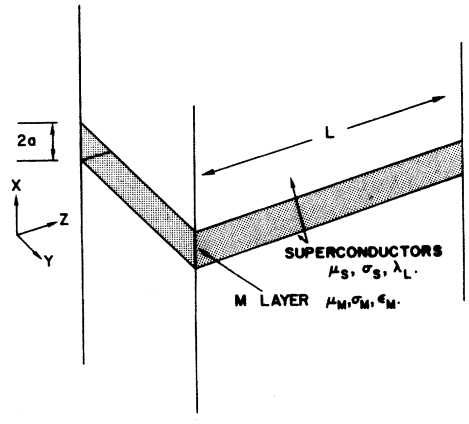

FIG. 1. Geometry of the *SMS* Josephson junction, where *S* denotes a superconductor and *M*, the middle layer, is either an insulator or a normal metal. Either the *S* or the *M* layer may contain the magnetic system.

where $\mathbf{j}_N$ is the normal current density given by Ohm's law

$$\mathbf{j}_N=\sigma\mathbf{E}\,, \tag{2.4}$$

$\mathbf{j}_S$ is the superconducting current density given by the London equations[12]

$$\mathbf{j}_S=-\frac{1}{\mu_0\lambda_L^2}\mathbf{A}\,, \tag{2.5a}$$

$$\frac{\partial\mathbf{j}_S}{\partial t}=\frac{1}{\mu_0\lambda_L^2}\mathbf{E}\,, \tag{2.5b}$$

$$\nabla\cdot\mathbf{A}=0\,, \tag{2.5c}$$

and $\mathbf{j}_J$ is the Josephson current density given by the Josephson equation[13]

$$\mathbf{j}_J=\mathbf{J}_c\sin\phi\,. \tag{2.6}$$

In Eqs. (2.4)–(2.6), σ is the electrical conductivity,

$$\mu_0=4\pi/10^7\,,$$

is the permeability of free space, λ_L is the London penetration depth, $\mathbf{A}$ is the magnetic vector potential, $\mathbf{J}_c$ is the Josephson critical current density, and ϕ is the phase difference between the Cooper pair wave functions in the two *S* layers. The temporal and spatial dependences of ϕ are given by

$$\frac{\partial\phi}{\partial t}=\frac{2eV}{\hbar}\,, \tag{2.7}$$

$$\nabla\phi=\frac{2ed}{\hbar}(\mathbf{B}\times\hat{\mathbf{n}})\,. \tag{2.8}$$

Here V is the electrical potential difference across the junction, $\hat{\mathbf{n}}$ is the unit vector in the x direction, and

$$d\equiv 2(a+\lambda)\,, \tag{2.9}$$

λ being the actual penetration depth which, as we will show later, is related to the London penetration depth λ_L by

$$\lambda=\left[\frac{\mu_0}{\mu_S}\right]^{1/2}\lambda_L\,, \tag{2.10}$$

where μ_S is the magnetic permeability of the *S* layers.

For a voltage V_0 applied along the x direction and a magnetic field H_0 applied along the y direction, from Eqs. (2.7) and (2.8),

$$\left[\frac{\partial\varphi}{\partial t}\right]_0=\frac{2eV_0}{\hbar}\equiv\omega_0\,, \tag{2.11a}$$

$$\left[\frac{\partial\varphi}{\partial z}\right]_0=\frac{2ed\mu_0H_0}{\hbar}\equiv k_0\,. \tag{2.11b}$$

In solving the Maxwell equations (2.1) and (2.2), we assume the media to be isotropic so that

$$\mathbf{D}=\epsilon\mathbf{E} \tag{2.12}$$

and

$$\mathbf{B}=\mu\mathbf{H}\,. \tag{2.13}$$

We also make a Fourier transformation in time by setting

$$\frac{\partial}{\partial t}\rightarrow i\omega \ .$$

The Maxwell equations thus reduce to

$$\nabla\times\mathbf{E}=-i\omega\mu\mathbf{H} \ , \tag{2.14}$$

$$\nabla\times\mathbf{H}=\left[i\omega\epsilon+\sigma-\frac{i}{\omega\mu_0\lambda_L^2}\right]\mathbf{E}+\mathbf{j}_J=\sigma_c\mathbf{E}+\mathbf{j}_J \ , \tag{2.15}$$

where

$$\sigma_c\equiv i\omega\epsilon+\sigma-\frac{i}{\omega\mu_0\lambda_L^2} \ . \tag{2.16}$$

Combining the two equations (2.14) and (2.15) and using the Maxwell equation

$$\nabla\cdot\mathbf{B}=0 \ , \tag{2.17}$$

we obtain

$$\nabla^2\mathbf{H}=i\omega\mu\sigma_c\mathbf{H}+\nabla\times\mathbf{j}_J \ . \tag{2.18}$$

Since the Josephson current is taken to be along the x direction,

$$\nabla\times\mathbf{j}_J=\frac{\partial j_J}{\partial z}\hat{\mathbf{m}} \ , \tag{2.19}$$

where $\hat{\mathbf{m}}$ is a unit vector in the y direction. Equation (2.18) thus reduces to

$$\nabla^2\mathbf{H}=i\omega\mu_M(i\omega\epsilon_M+\sigma)\mathbf{H}+\frac{\partial j_J}{\partial z}\hat{\mathbf{m}} \tag{2.20}$$

for the M layer and to

$$\nabla^2\mathbf{H}=i\omega\mu_S\left[i\omega\epsilon_S+\sigma-\frac{i}{\omega\mu_0\lambda_L^2}\right]\mathbf{H} \ , \tag{2.21}$$

with no inhomogeneous term, for the S layers.

In order to find the solutions to these equations we follow the normal procedure of first solving the homogeneous problem and then expressing the solution to the inhomogeneous equation as an expansion in terms of the homogeneous solutions, with the coefficients determined by the usual methods.

We look for separable solutions of the form

$$H=H_n(x)e^{ik_nz} \ , \tag{2.22}$$

which amounts to making a Fourier transformation $\partial/\partial z\rightarrow ik_n$ for the z direction, and in keeping with our geometry, assumes that there is no y dependence of H, i.e., $\partial/\partial y\rightarrow 0$.

For the M layer, the homogeneous part of Eq. (2.20) reduces to

$$\left[\frac{\partial^2}{\partial x^2}-k_n^2+\frac{\omega^2}{c^2}-i\frac{2}{\delta^2}\right]H_n=0 \ , \tag{2.23}$$

where we have substituted the skin depth

$$\delta\equiv\left[\frac{2}{\sigma\omega\mu_M}\right]^{1/2} \tag{2.24}$$

and the velocity of light c in the M layer (in the absence of the S layers):

$$c=(\mu_M\epsilon_M)^{-1/2} \ . \tag{2.25}$$

For the S layers, the first two terms in (2.15), corresponding to the displacement and the normal currents, can be ignored compared to the third (the superconducting) term and Eq. (2.20) reduces to

$$\left[\frac{\partial^2}{\partial x^2}-k_n^2-\frac{\mu_S}{\mu_0\lambda_L^2}\right]H_n=0 \ . \tag{2.26}$$

We may assume solutions to Eqs. (2.23) and (2.26) of the forms

$$H_n^M=\frac{h_n}{2}\left[\exp\left[\frac{x-a}{\Delta}\right]+\exp\left[\frac{-x+a}{\Delta}\right]\right], \quad -a<x<a \ , \tag{2.27}$$

$$H_n^{S1}=h_n\exp\left[\frac{-x-a}{\lambda}\right], \quad x>a \ , \tag{2.28}$$

$$H_n^{S2}=h_n\exp\left[\frac{x+a}{\lambda}\right], \quad x<-a \ , \tag{2.29}$$

for the M and the upper and the lower S layers, with quantities h_n, Δ, and λ to be determined. To determine λ, it is assumed that $(k_n\lambda)^2\ll 1$ whence, from (2.26), $\lambda=(\mu_0/\mu_S)^{1/2}\lambda_L$ justifying (2.10). Trivially, the boundary condition for the continuity of the tangential components of the $\mathbf{H}$ field at the interfaces $x=\pm a$ is satisfied if $a\ll\Delta$, which will later be shown to be valid. The next boundary condition to be satisfied is the continuity of the tangential component of the $\mathbf{E}$ field at the interfaces $x=\pm a$. From Eq. (2.15) with $\mathbf{j}_J=0$,

$$\nabla\times\mathbf{H}=\sigma_c\mathbf{E} \ , \tag{2.30}$$

which leads to

$$E_z=\frac{1}{\sigma_c}\frac{\partial H}{\partial x} \ . \tag{2.31}$$

Equations (2.27)–(2.31) and the continuity requirement of E_z at the interfaces give a relation between Δ and λ:

$$\frac{1}{\Delta^2}=\frac{\mu_S\lambda}{\mu_M a}K^2 \ , \tag{2.32}$$

where

$$K\equiv\left[\frac{\omega^2}{c^2}-\frac{2i}{\delta^2}\right]^{1/2} \ . \tag{2.33}$$

The substitution of (2.27) and (2.32) back into (2.23) results in the dispersion relation for the junction

$$\omega_n=c\left[\frac{a}{b}k_n^2+i\frac{2}{\delta^2}\right]^{1/2} \ , \tag{2.34}$$

where

$$b\equiv\frac{\mu_S\lambda+\mu_M a}{\mu_M} \ . \tag{2.35}$$

It is easy to make a connection with the usual result for an undoped *SIS* junction. In this case $\mu_S \sim \mu_M \sim \mu_0$ and for $\delta \to \infty$ Eq. (2.34) reduces to

$$\omega_n = \bar{c} k_n \ , \tag{2.36}$$

where

$$\bar{c} \cong c \left[\frac{2a}{d} \right]^{1/2} \tag{2.37}$$

is the standard result for the reduced speed of light in such a structure.[14] The more general result (2.34) accounts for damping via the normal conduction term $2i/\delta^2$. Somewhat hidden, but of importance here, are the imaginary contributions to ω_n which arise because in general μ_S and μ_M contain the complex dynamic susceptibilities of the dopants.

Finally, in connection with the solutions of the homogeneous problem, we must specify the boundary conditions at the ends of the junction, $z = \pm L/2$, which determine the allowed vectors k_n. In principle, the continuity of **E** and **H** at these ends requires a coupling between the internal and the external modes of the system, e.g., standing waves in the feeding wires, and makes the problem too complicated. However, as was shown above, the speed of light $\bar{c}$ in the *SMS* structure is much smaller than that outside the junction. As a result, it is reasonable to assume that the electromagnetic waves are almost totally reflected at $z = \pm L/2$. This assumption drastically simplifies the problem. It implies that E_x vanishes at $z = \pm L/2$, whence $E_x(z,t)$ may be expanded in a Fourier series

$$E_x(z,t) = \sum_{\text{even } n} E_n(t) \sin(k_n z) + \sum_{\text{odd } n} E_n(t) \cos(k_n z) \ , \tag{2.38}$$

where

$$k_n = \frac{n\pi}{L} \tag{2.39}$$

and n is an integer. Since **E** and **H** are interrelated via the Maxwell equations it follows that (2.39) for k_n determines the allowed values in (2.34) for ω_n. This completes the solution of the homogeneous problem.

Next we turn to the inhomogeneous problem. So far, this problem has not been fully specified since a detailed prescription for the phase ϕ in Eq. (2.6) has not been given. We shall write

$$\phi(z,t) = kz + \frac{2e}{\hbar} \int_0^t dt V(z,t) \equiv kz + \omega t + \Phi(z,t) \ , \tag{2.40}$$

where $V = 2aE_x$ is the potential difference across the junction. This formula, which has been used by a number of authors, directly implies that the phase difference ϕ couples to electric field fluctuations in the M layer. Goldman *et al.*[6] use instead

$$\Phi(z,t) = \left[\frac{2ed}{\hbar} \right] \int dz' M_y(z',t) + \left[\frac{2ed}{\hbar} \right] \int dt' \int dz' \frac{\partial M_y}{\partial t}(z',t) \ . \tag{2.41}$$

The last term can be obtained from Eq. (2.7), using Faraday's law and is equivalent to our (2.40). By contrast, the first term is obtained by integration of Eq. (2.8)

$$\frac{\partial \phi}{\partial z} = \frac{2ed}{\hbar} B_y(z,t) = \frac{2ed}{\hbar} (\mu_0 H + M_y) \tag{2.42}$$

and implies that ϕ couples directly to fluctuations in the magnetization **M**. However, mathematically it is incorrect to integrate *both* Eqs. (2.7) and (2.8) and *add* the resulting terms involving M_y. In fact, we may integrate *either* of these equations and show that the two answers agree by using the Maxwell equations. Our expression Eq. (2.40) correctly accounts for *both* electric field and magnetization fluctuations.

To find a particular integral of the inhomogeneous equations we expand the field in terms of the homogeneous solutions (in complex notation):

$$H(x,z,t) = \sum_{n'} H_{n'}(x) e^{i(\omega t + k_{n'} z)} \ , \tag{2.43}$$

where the coefficients in the expansion are the H_n in Eqs. (2.27)–(2.29). We then substitute the zeroth-order formula for the Josephson current

$$j_J = J_c \sin(\omega_0 t + k_0 z) \tag{2.44}$$

into Eq. (2.20). If we multiply Eq. (2.20) by $e^{-i(\omega t + k_n z)}$ and integrate z over the length of the junction, we find

$$\left[\frac{1}{\Delta^2} - k_n^2 + \frac{\omega^2}{c^2} - i\frac{2}{\delta^2} \right] h_n = -ik_n j_n \ , \tag{2.45}$$

where we have used

$$\frac{\partial^2}{\partial x^2} \to -\frac{1}{\Delta^2}$$

and where

$$j_n = J_c S_n \ . \tag{2.46}$$

The "overlap" coefficients S_n are given by

$$S_n \equiv \frac{1}{L} \frac{4k_n}{k_0^2 - k_n^2} \sin(k_0 - k_n) \frac{L}{2} \ . \tag{2.47}$$

For $\Delta \gg a$, the x dependence of $H_n(x)$ is negligible and so one can equate H_n and h_n, i.e.,

$$H_n = h_n = \frac{-ik_n j_n}{(b/a)K^2 - k_n^2} \ . \tag{2.48}$$

From Eqs. (2.48) and (2.15),

$$E_{xn} = \frac{i\omega\mu_M}{K^2 - (a/b)k_n^2} j_n \ . \tag{2.49}$$

We rewrite Eq. (2.49) in the complex notation

$$E_{xn} = i\omega\mu_0 A_n e^{i\theta_n} j_n \ , \tag{2.50}$$

where A_n and θ_n are real and determined from Eq. (2.49).

We now combine Eqs. (2.38), (2.46), and (2.50) and obtain

$$E_x(z,t)=J_c\omega\mu_0\left[\sum_{\text{odd }n} S_nA_n\cos(\omega t+\theta_n)\cos(k_nz) - \sum_{\text{even }n} S_nA_n\sin(\omega t+\theta_n)\sin(k_nz)\right] \tag{2.51}$$

for the time-dependent component of E_x.

Equation (2.51) represents the completion of one iteration in the search for a self-consistent solution of our basic equations. The self-consistent nature of the problem arises because the time-dependent electric potential difference produced by $E_x(z,t)$ across the barrier is

$$V(z,t)=2aE_x(z,t)\ . \tag{2.52}$$

In principle we should set

$$V=V_0+v \tag{2.53}$$

in Eq. (2.40) for $\phi(z,t)$ and repeat the steps following Eq. (2.44). However, for the present purposes, the first iteration which gives (2.51) is sufficient to calculate the electromagnetic response of the junction. One finds for ϕ,

$$\phi=\omega_0t+\frac{4ea}{\hbar}\mu_0J_c\xi\ , \tag{2.54}$$

where

$$\xi\equiv\sum_{\text{even }n} S_nA_n\sin(\omega_0t+\theta_n)\cos(k_nz) + \sum_{\text{odd }n} S_nA_n\cos(\omega_0t+\theta_n)\sin(k_nz)\ , \tag{2.55}$$

and from the Josephson Eq. (2.6), expanding in J_c,

$$j_J=J_c\sin(\omega_0t+k_0z)+\frac{4ea}{\hbar}\mu_0J_c^2\xi\cos(\omega_0t+k_0z)\ . \tag{2.56}$$

Integrating Eq. (2.56) over the junction and averaging over time gives the dc current

$$I=J_0\sum_{n=1}^{\infty} S_n^2A_n\sin\theta_n\ , \tag{2.57}$$

where

$$J_0\equiv 2eaW\mu_0J_c^2/\hbar \tag{2.58}$$

and W is the area of the junction.

Equation (2.57) is the principal, but rather formal, result of this section. Physically interesting results are obtained through the evaluation of A_n and θ_n defined by comparison of Eqs. (2.49) and (2.50). The properties of the all important magnetic systems are introduced via the complex dynamical magnetic susceptibility in the Fourier space:

$$\chi(\mathbf{q},\omega)=\chi'-i\chi''=\frac{\mu}{\mu_0}-1\ . \tag{2.59}$$

The wave vector $\mathbf{q}$ entering the χ argument is determined by Eqs. (2.27)–(2.29)

$$\mathbf{q}_M\cong\left[\pm\frac{i}{\Delta},0,k_n\right]\ , \tag{2.60}$$

$$\mathbf{q}_S\cong\left[\pm\frac{i}{\lambda},0,k_n\right]\ . \tag{2.61}$$

It is important to realize that the wave vector probed is one of the wave vectors obtained by imposing boundary conditions upon the electric field but that this wave vector has an imaginary x component corresponding to the fact that the magnetic field decays exponentially in this direction. The wave vector in the M layer and most of the remaining results depend upon whether this is an insulator or a metal.

If the barrier is an insulator,

$$a\ll\lambda,\quad \sigma\to 0\ ,$$

and from Eqs. (2.32)–(2.35),

$$\frac{1}{\Delta_I}\sim k_n\ . \tag{2.62}$$

Since the imaginary x component of $\mathbf{q}$ in the I layer is of the same order of magnitude as the z component, the concept of wave vector in an I layer is ill defined. However, if the barrier is a normal metal,

$$a\gg\lambda,\quad \sigma \text{ large}$$

and

$$\frac{1}{\Delta_N}\ll k_n\ . \tag{2.63}$$

So the concept of a wave vector in a normal-metal barrier is rather well defined.

Whatever the M layer, in the S layer, the imaginary part

$$\frac{1}{\lambda}\sim 10^7\ \text{m}^{-1}\ .$$

Therefore, the wave vector is well defined if k_n is large compared to this value. The imaginary parts of the wave vectors do not occur in the simpler approach of Goldman *et al.*[6]

From Eqs. (2.49), (2.50), and (2.57),

$$I=J_0\sum_{n=1}^{\infty} S_n^2\text{Im}\left[\frac{\mu_0}{\mu_M}\left[\frac{\omega_0^2}{c^2}-\frac{2i}{\delta^2}\right]-\frac{a\mu_0k_n^2}{\mu_S\lambda+\mu_Ma}\right]^{-1}\ . \tag{2.64}$$

For an *SIS* junction, $\sigma\to 0$, $a\ll\lambda$, and Eq. (2.64) reduces to

$$I_{SIS}\cong J_0\sum_{n=1}^{\infty} S_n^2\text{Im}\left[\frac{\mu_0}{\mu_I}\frac{\omega_0^2}{c^2}-\frac{a\mu_0k_n^2}{\mu_S\lambda}\right]^{-1}\ . \tag{2.65}$$

If the I layer is magnetically doped, $\mu_S\to\mu_0$, and Eq. (2.65) gives

$$I_1\cong I_0\sum_{n=1}^{\infty} S_n^2\frac{\chi''}{(1-f_n)^2+(\chi'')^2}\ , \tag{2.66}$$

where

$$I_0\equiv J_0\frac{\lambda_L}{a}\left[\frac{\bar{c}}{\omega_0}\right]^2$$

and

$$f_n \equiv \left[\frac{\omega_n}{\omega_0}\right]^2 .$$

If the S-layer is magnetically doped, $\mu_I \to \mu_0$, and (2.65) gives

$$I_2 \sim I_0 \sum_{n=1}^{\infty} S_n^2 \frac{f_n \chi''/2}{(1-f_n)^2+(f_n\chi''/2)^2} . \tag{2.67}$$

For an SNS junction, $a \gg \lambda$, and the displacement term in Eq. (2.64) can be ignored compared to the conduction term, i.e., $\omega_0^2/c^2 \ll 2/\sigma^2$ and Eq. (2.64) reduces to

$$I_{SNS} = J_0 \sum_{n=1}^{\infty} S_n^2 \mathrm{Im}\left[\frac{\mu_0}{\mu_N}\left[-\frac{2i}{\delta^2}-k_n^2\right]\right]^{-1} . \tag{2.68}$$

If we make the substitutions

$$\frac{\mu_N}{\mu_0} \to 1+\chi'-i\chi''$$

and

$$\frac{1}{\delta^2} \to \frac{1}{\delta_0^2}(1+\chi'-i\chi'') ,$$

where δ_0 is the skin depth in the absence of the magnetic dopants, Eq. (2.68) reduces to

$$I_3 \cong I_0' \sum_{n=1}^{\infty} S_n^2 \left[\frac{2+p_n\chi''}{[p_n(1-\chi')]^2+(2+p_n\chi'')^2}\right] , \tag{2.69}$$

where $I_0' \equiv J_0\delta_0^2$ and $p_n \equiv \delta_0^2 k_n^2$.

Since the expression between the brackets in Eq. (2.69) is a slowly varying function of k_n, the overlap function S_n^2 acts as an explicit δ function and for the SNS junction for an applied magnetic field, such that $k_0 = q \cong k_N$, it is possible to make the simplification

$$I_3 \cong I_0' \frac{2+p_N\chi''}{[P_N(1+\chi')]^2+(2+p_N\chi'')^2} . \tag{2.70}$$

A similar approximation is *not* valid for the SIS junctions since both terms in the sum are sharply peaked.

Our final results for this section are Eqs. (2.66) or (2.67) for the SIS junction, depending on whether the insulator or the superconductor is magnetically doped, while the somewhat simpler Eq. (2.70) is relevant for the SNS junctions with the N layer magnetically doped.

III. SPECTROSCOPIC RESPONSE

In this section, we first estimate the size of the magnetic signal for the simple SMS junction on the basis of the theory developed in Sec. II, and then discuss the possible merits of more complicated $SINS$ and $SISN$ structures. Next, we outline the theory for a single-point contact SNS and two-point contact (or SQUID) arrangements and relate the theoretical results to the recent experiments of Baberschke *et al.*[5]

In the absence of saturation, the magnetic system can be represented by a complex rf susceptibility[15]

$$\chi(q,\omega) = \chi' - i\chi'' = \chi_0 \left[\frac{\omega_s(\omega_s-\omega)-i\omega_s\Delta\omega_s}{(\omega_s-\omega)^2+(\Delta\omega_s)^2}\right] , \tag{3.1}$$

where χ_0 is the static susceptibility and the resonant frequency ω_s may contain zero-field, Zeeman, and magnon-dispersion terms

$$\omega_s = \omega_c + \omega_Z + \omega_m , \tag{3.2}$$

where the zero-field term ω_c may be caused by the crystal-field or electron-nuclear interactions giving rise to fine or hyperfine structures, respectively; ω_Z is the Zeeman interaction with an applied magnetic field H_0

$$\hbar\omega_Z = \mu_B g H_0 , \tag{3.3}$$

where μ_B is the Bohr magneton and g is the ratio of the magnetic moment to the angular momentum of the magnetic centers. For an antiferromagnet, the magnon term ω_m may be written as

$$\omega_m = vq \tag{3.4}$$

where v is the magnon velocity ($v \ll c$).

The experiments to date[5] have involved dilute magnetic alloys, where only the ω_c term is important and $\Delta\omega_s$ is primarily due to the Korringa[16] relaxation. If one considers more complicated systems such as spin-glasses of antiferromagnets, the magnon term ω_m becomes important.

The width $\Delta\omega_s$ arises from diverse sources. For example, in the above experiments[5] it was due to inhomogeneous broadening in addition to the Korringa relaxation. For a spin-glass, a ferromagnet or an antiferromagnet, hydrodynamic theory would suggest a diffusion term Dq^2.

A. *SIS* junctions

For an SIS junction doped with magnetic impurities, the relevant equations are (2.66) and (2.67). These equations together with Eq. (3.1) lead to three types of maxima in I_{dc}: (a) The self-resonant or Fiske modes[9] which occur at

$$\frac{2e}{\hbar}V_0 \equiv \omega_0 = \omega_n = \bar{c}k_n \equiv \bar{c}\frac{n\pi}{L} . \tag{3.5}$$

(b) The peaks in the overlap function S_n^2 which occur at

$$\frac{2ed}{\hbar}H_0 \equiv k_0 = k_n \equiv \frac{n\pi}{L} . \tag{3.6}$$

When the individual Fiske modes are not resolved, the intensity of their envelope becomes magnetic field dependent and is known as the Eck mode,[7] (c) when ω_0 is not close to ω_n:

$$I_{dc} \propto \chi''$$

and magnetic resonances appear at

$$\omega_0 = \omega_s . \tag{3.7}$$

Equations (3.5) and (3.7) show that the Josephson frequency ω_0 corresponding to the applied voltage V_0 must be compared with both the magnetic resonance frequency ω_s and the frequency ω_n for Fiske modes. Similarly, the Josephson wave vector k_0 corresponding to the applied

field H_0 must be compared with both the desired wave vector q and the k_n, again associated with the Fiske modes.

For a junction of length L of the order of 10 μ, the first Fiske mode ω_1 is $\sim$1000 GHz. The frequency ω_s for small wave vectors q is typically of the order of a few GHz and is well below the first Fiske mode. In such a situation the Fiske modes are safely out of the picture. We would then like to select a given wave vector q by adjusting the applied field such that

$$k_0 = q \ .$$

However, the coupling is not direct between the Josephson current and the magnetic system, but rather it is via the intermediary of the Fiske modes, which in the above-described situation are, by design, driven well below their resonances.

Under such circumstances, one must ask which value or values of n dominate the sums in (2.66) and (2.67). To this end, it is instructive to compare the magnitude of the $n=1$ term with that of the $n=N$ term for which

$$k_0 = q \cong k_N \ ,$$

i.e., the Nth Fiske mode has its wave vector (which is approximately equal to the desired wave vector q) matched to the external field.

If the dimension L of the junction is such that the first Fiske mode is larger than the desired frequencies, i.e.,

$$\omega_0 = \omega_s < \omega_1 \ ,$$

and if χ'' is small compared to unity, Eqs. (2.66) and (2.67) simplify to

$$I_1 \sim I_0 \sum_{n=1}^{\infty} S_n^2 \frac{\chi''}{f_n^2} \tag{3.8}$$

and

$$I_2 \sim I_0 \sum_{n=1}^{\infty} S_n^2 \frac{\chi''}{2f_n} \ . \tag{3.9}$$

The coefficient S_n^2 for the two cases $n=1$ and $n=N$, determined from the definition (2.47) by putting $k_0 = k_N$, are

$$S_1^2 \sim \frac{1}{N^4}$$

and

$$S_N^2 \sim 1 \ .$$

From the definition $f_n \equiv (\omega_n/\omega_0)^2$,

$$f_N = N^2 f_1 \ .$$

Therefore, if the I layer is magnetically doped, from Eq. (3.8)

$$(I_1)_{n=1} \cong (I_1)_{n=N} \rightarrow I_0 \frac{\chi''}{N^4 f_1^2} \ .$$

Thus, the net signal which derives from the low $n \sim 1$ Fiske modes is comparable with those which arise from the field-matched mode $n \sim N$ and the observed signal will correspond to a mixture rather than a single wave vector. Furthermore, as shown in Sec. II, the wave vector q in this case has a large imaginary part and hence is ill defined. However, this ill-defined wave vector is not a problem. This is because the I layer is very thin and the x component of the magnon wave vector must satisfy some boundary condition. The coupling to such different wave vectors will be determined by an overlap integral which will only be appreciable for magnon wave vectors of vanishing x component. Hence, *for a given* k_n, the wave vector of the magnons is perfectly well defined even though that of the magnetic field is not. However, since many values of k_n are involved, *SIS* junctions with doped I layers are not suitable for determining the magnon dispersion relations.

In contrast, if the impurity is in the S layer, from Eq. (3.9),

$$(I_2)_{n=N} \cong N^2 (I_2)_{n=1} \rightarrow I_0 \frac{\chi''}{N^2 f_1}$$

and, therefore, the observed signal *is* determined by the field-matched mode. The study of the magnon dispersion relation is, thus, possible if the magnetic system under investigation is in the S layer. Furthermore, as discussed in Sec. II, the concept of the wave vector *is* meaningful in the S layer if q is large compared to the inverse penetration depth in the S layer. Since $\lambda \sim 10^{-7}$ m, this implies quite large wave vectors. However, provided that the S layer is sufficiently thin, the boundary condition will determine the x component of the wave vector as described above. Under such circumstances the S layer exhibits two-dimensional behavior.

Although an *SIS* junction, with the magnetic system in the I layer, is unsuitable for the study of the magnon dispersion relation, it is suitable for the detection of *dilute* impurity ESR. Furthermore, bulk nuclear magnetic resonance is a possibility, since at realistic temperatures the nuclei have no significant k dependence. In such experiments, the value of the applied magnetic field may be optimized by adjusting k_0 such that

$$k_0 \cong k_1 \ ,$$

and from Eq. (3.8) the signal is estimated via

$$I_1 = I_0 \left[\frac{\omega_s}{\omega_1} \right]^4 \chi'' \ , \tag{3.10}$$

i.e., the maximum signal is obtained when $\omega_s/\omega_1 \rightarrow 1$ and

$$I_1 \rightarrow J_0 \left[\frac{\lambda}{a} \right] \left[\frac{L}{\pi} \right]^2 \chi'' \ .$$

If the applied field H_0 is much larger than its optimal value, e.g, as might be the case if it is adjusted to satisfy the resonance condition (3.7), the signal decreases as $(H_1/H_0)^{-2}$, where H_1 is the value satisfying the condition $k_0 = k_1$.

Since $J_0 L^2$ is $\sim I_c$, the critical current of the junction, simple estimates (see Sec. IV) suggesting a magnetic response of the order of I_c will be possible for a concentration of magnetic ions as low as 0.1%. Under favorable

conditions, concentrations as low as 1 ppm should be detectable. The precise response, however, depends upon the details of the magnetic resonance and in particular on the width of the ESR line.

B. *SNS* junctions

For an *SNS* junction, the relevant expressions are Eqs. (2.69) and (2.70). First, we must discuss the region of validity of the perturbation approach used to derive these expressions. For a resistively shunted Josephson junction[17] of small capacitance and in the absence of a magnetic system, the current and voltage are related by

$$V=(I^2-I_c^2)^{1/2}R \ .$$

For $V>I_cR$,

$$I\cong\frac{V}{R}+\frac{1}{2}\left[\frac{I_cR}{V}\right]I_c=\frac{V}{R}+I_{\rm dc} \ . \tag{3.11}$$

From Eq. (2.70) for a nonmagnetic system,

$$I_3=I_{\rm dc}\cong\tfrac{1}{2}J_0\delta_0^2=\frac{1}{2}\left[\frac{2ea\mu_0I_c\delta_0^2}{\hbar}\right]I_c\equiv\tfrac{1}{2}\eta I_c \ . \tag{3.12}$$

In arriving at Eq. (2.57) from Eq. (2.56) we assumed that η was small compared to unity. A comparison of Eqs. (3.11) and (3.12) shows that our results are valid for

$$V\geq I_cR \ .$$

With this proviso, Eq. (2.70) may be rewritten in the form

$$I_3=I_{\rm dc}=I_c\left[\frac{I_cR}{V}\right]\frac{2+p_N\chi''}{[p_N(1-\chi')]^2+(2+p_N\chi'')^2} \ . \tag{3.13}$$

If one is interested in measuring the wave-vector-dependent dynamic susceptibility $\chi(q,\omega)$, the applied magnetic field must be adjusted such that

$$k_0=q\sim k_N \ .$$

For

$$p_N=(q\delta_0)^2\gg\chi\leq 1 \ ,$$

Eq. (3.13) simplifies to

$$I_{\rm dc}=I_c\left[\frac{I_cR}{V}\right]\frac{\chi''(q,\omega)}{(q\delta_0)^2} \ . \tag{3.14}$$

When the interest is in the ESR of dilute alloys with a zero-field splitting, a small field, such that

$$k_0=k_1 \ ,$$

will suppress the dc critical current making the I-V curve more linear and optimize the coupling of the current to the $n=1$ mode. In Eq. (3.13), setting

$$p_1=(k_1\delta_0)^2\sim 1$$

and

$$I_cR\sim V \ ,$$

gives

$$I_{\rm dc}\sim I_c[\alpha\chi'(\omega)+\beta\chi''(\omega)] \ , \tag{3.15}$$

with α and β of the order of unity determined by the precise value of p_1.

C. *SISN* and *SINS* junctions

We have solved the problem of symmetric *NSISN* junctions where the S layers have a thickness t. The calculations are quite lengthy. However, the results are readily appreciated on physical grounds and for this reason the derivation will not be given.

We are interested in the situation where the N layer(s) contain the magnetic system. What is required is a dispersion relation, i.e., a modification of Eq. (2.34) which via Eq. (2.50) determines A_n and θ_n.

First consider the case where the penetration depth $\lambda\gg t$. In this case, apart from generating the Josephson effect, the S layers play no role. Consider again Eq. (2.34) for a simple *SIS* junction, with the I-layer conductivity zero. Since with our approximation of ignoring the normal current in the S layers they are lossless, the resulting dispersion relation

$$\omega_n^2=\left[\frac{a}{\lambda}\right]c^2k_n^2$$

represents undamped propagation. In contrast in an *NSISN* junction, this is no longer true. In the limit

$$a\ll\delta, \quad t\ll\lambda \ ,$$

the dispersion relation becomes

$$\omega_n^2=(1-i)\left[\frac{\mu_0a}{\mu_N\delta}\right](k_nc)^2 \ , \tag{3.16}$$

i.e., the characteristic frequencies are heavily damped with equal real and imaginary parts.

The final result for $I_{\rm dc}$ is of the form (2.66) and (3.10) with

$$\lambda\to\delta, \quad \chi''\to\chi''+\chi', \quad \mathbf{q}\cong\left[\frac{i}{\delta},0,k_n\right] \ ,$$

and as with conventional ESR in metals, there is an equal admixture of absorption and dispersion in the measured response.

In the inverse situation where

$$t\gg\lambda \ ,$$

we find

$$\omega_n^2\cong\left[\frac{a}{\lambda}+4(1-i)\left[\frac{\mu_0a}{\mu_n\delta}\right]e^{-2t/\lambda}\right](k_nc)^2 \ . \tag{3.17}$$

Now Eqs. (2.66) or (3.10) may be used *without* replacing λ by δ and with

$$\chi''\to(\chi''+\chi')4e^{-2t/\lambda} \ .$$

In essence, apart from numerical factors of order unity, both cases can be represented by (3.17); as the superconductor layer thickness is increased, the coupling to the ex-

terior N layer is diminished exponentially. Because of the second term in the brackets in (3.17), for small values of t the Fiske modes become very strongly damped. In fact, the response predicted by (2.66) will be similar to that for an *SNS* junction described by (2.70). Increasing the S-layer thickness permits this response to be varied continuously between *SNS* and *SIS* behaviors. Clearly, again to within numerical factors of order unity, the removal of one N layer to leave an *SISN* structure would not change Eqs. (3.16) and (3.17).

Such *SISN* structures have the obvious advantage of not requiring the magnetic system to be contained in either the barrier or the S layers where it may destroy the Josephson effect. Furthermore, they offer the possibility of varying the coupling of the magnetic system and have obvious advantages from the fabrication point of view.

The alternative *SINS* ordering of the layers offer similar possibilities of interpolating between *SIS* and *SNS* behavior but it is more difficult to vary the coupling to the magnetic system. The theory is essentially the same as that in Sec. II, except that the conductivity and susceptibility (assuming that the magnetic system is in the N layer) are "diluted" by the ratio t/a of the N layer to the total barrier thickness. Including an I layer in an *SNS* junction might be a useful way of controlling the critical current independently of the normal layer thickness and thereby might constitute a way of tuning the I_cR product to the desired value, i.e., $\hbar\omega \sim eI_cR$ [see the discussion following Eq. (3.12)].

D. Point-contact *SNS* junctions

Here we envisage the physical structure illustrated in Fig. 2(a). A more or less sharp point is brought into contact with an *NS* planar sandwich. If the dimension L of the tunneling region under the point is greater than the skin depth δ, then the junction can be considered in the same way as the *SNS* junctions of the preceding sections. However, when $L \ll \delta$ it is more appropriate to consider the junction region as a line of oscillating current screened by currents flowing in the N layer.

To make an easily tractable problem requires a fair degree of abstraction and several assumptions about the form of the point-N-layer contact. These assumptions are illustrated in Fig. 2(b). The tunneling current which now flows in the z direction is envisaged as occupying a circular region of diameter L. The N layer has a uniform thickness $2a$. There are superconductors both above and below it in normal (or perhaps more realistically strong capacitive) contact. The aim of these assumptions is to reduce the problem to one with cylindrical symmetry. In particular, the assumption about the nature of the S-N contact away from the central region is a crude approximation. For this reason the present calculations are only intended to illustrate the various factors involved.

Keeping only the normal current and using complex notation for an ac effect of frequency ω, we have from (2.20)

$$\frac{d^2H}{dr^2}+\frac{1}{r}\frac{dH}{dr}-\frac{1}{r^2}H-\frac{2i}{\delta^2}H=0\ , \tag{3.18}$$

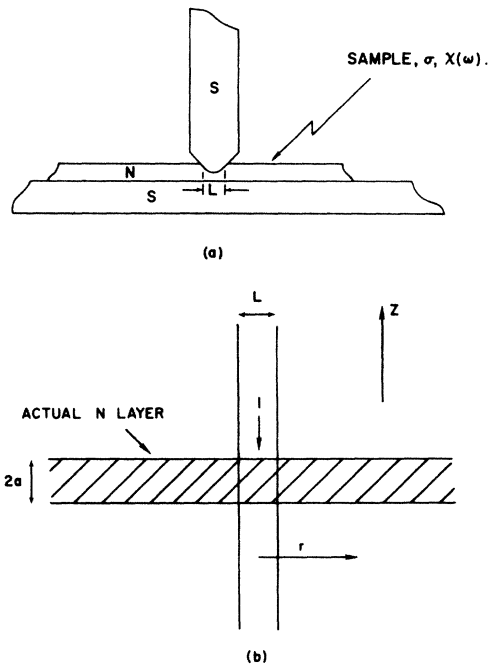

FIG. 2. (a) Geometry for the pont-contact *SNS* junction. The dimension L is that of the region where the Josephson current flows. (b) The idealized, cylindrically symmetric geometry used in the calculations. It is assumed that there is a cylinder in which the Josephson current, $I=I_c\sin(\omega t)$, flows. The shaded N-layer region has a normal conductivity σ and contains magnetic impurities. The potential difference across the junction is assumed to be that between the top and the bottom of the shaded layer at a radius $r=L/2$.

which is Bessel's equation with $n=1$. The relevant solution is the Hankel function $H_1^{(1)}(z)$ where $z=\kappa r$ and $\kappa=-(1-i)/\delta$.

Ampere's law gives $H(L/2)=I_c/\pi L$ to yield

$$H(r)=-(I_c\kappa/4)H_1^{(1)}(\kappa r)\ . \tag{3.19}$$

Taking the curl gives

$$E_z(r)=-(I_c\kappa^2/4\sigma)H_0^{(1)}(\kappa r)\ . \tag{3.20}$$

With $H_0^{(1)}=J_0+iY_0$, $J_0=1-\frac{1}{2}z^2+\cdots$ and $Y_0=(2/\pi)[\ln(\frac{1}{2}z)+\gamma]J_0$, where $\gamma\sim 0.577$ is the Euler-Mascheroni constant. Since $|\kappa(L/2)|\sim L/\delta<1$, by assumption, we obtain

$$E_z\left[\frac{L}{2}\right]\cong -(I_c\kappa^2/4\sigma)\{(2i/\pi)[\ln(\kappa L/4)+\gamma]+1\}\ , \tag{3.21}$$

where the magnetic system enters via κ:

$$\kappa^2=-(2i/\delta_0^2)[1+\chi'(\omega)-i\chi''(\omega)]\ . \tag{3.22}$$

Assuming the susceptibility is small and separating real and imaginary parts

$$E_z\left[\frac{L}{2}\right]\cong(I_c/\sigma\pi\delta_0^2)\left\{F-\frac{i\pi}{4}+\left[(F+1)\chi'+\left[\frac{\pi}{4}+1\right]\chi''\right]+i\left[(F+1)\chi''-\left[\frac{\pi}{4}+1\right]\chi'\right]\right\}\equiv E_z'+iE_z'' , \tag{3.23}$$

where $F=\ln|L/4\delta|+\frac{1}{2}\ln 2+\gamma$. In complex notation the time-dependent field $E_z(t)=-(E_z'+iE_z'')e^{i\omega t}$ corresponding to a real field $E_z(t)=[(E_z')^2+(E_z'')^2]^{1/2}\cos(\omega t+\theta_0)$ where $\tan\theta_0=E_z'/E_z''$. The quantity $2aE_z(L/2)$ corresponds to the ac voltage between superconductors. Adding this to the dc voltage, we get

$$\phi(t)=\frac{2e}{\hbar}\int V(t)dt$$
$$=\frac{2eV_0}{\hbar}+\left[\frac{2e}{\hbar\omega}\right](2a)[(E_z')^2+(E_z'')^2]^{1/2}\sin(\omega t+\theta_0) , \tag{3.24}$$

where the phase shift θ_0 is all important.

This expression, which includes the perturbing effects of the rf field, is put back into the standard expression for the Josephson current:

$$I=I_c\sin\phi(t)\equiv I_c\sin[\omega t+(I_cR''/V)\cos(\omega t+\theta_0)]$$
$$\sim I_c\sin\omega t+(I_c^2R''/V)\cos(\omega t)\cos(\omega t+\theta_0) , \tag{3.25}$$

which after taking the average, yields

$$I_{dc}=(I_c^2R''/V)\sin\theta_0 ,$$

where

$$\cos\theta_0=E_z'/[(E_z')^2+(E_z'')^2]^{1/2}=(2a/I_c)(E_z'/R'')$$
$$=(I_c^2R'/V)\left[F+(F+1)\chi'(\omega)+\left[\frac{\pi}{4}+1\right]\chi''(\omega)\right] \tag{3.26}$$

and $R'=(2a/\sigma\pi\delta^2)$ is the resistance of a region of radius equal to the skin depth about the point contact.

The mysterious looking logarithmic function in these expressions is easy to understand from the following argument: By Ampere's law the field surround the point,

$$H(r,t)=(I_c/2\pi r)\sin(\omega t) , \tag{3.27}$$

but only to a distance δ beyond which the field is screened in the usual way. From the Maxwell equation $\nabla\times\mathbf{E}=-\partial\mathbf{B}/\partial t$, the rf voltage at $r=L/2$ is

$$2aE\left[\frac{L}{2}\right]\sim 2a\omega\mu\int_\delta^{r=L/2}H(r)dr$$
$$=[\mu\omega(2aI_c/2\pi)\ln(L/2\delta)]\cos(\omega t)$$
$$\sim[I_cR'\ln(L/2\delta)]\cos(\omega t) , \tag{3.28}$$

which essentially reproduces (3.23) or (3.21).

The form of our result for *SNS* point contacts is therefore

$$I_{dc}=(I_c^2R/V)(L/2\delta_0)^2[\alpha\chi'(\omega)+\beta\chi''(\omega)] , \tag{3.29}$$

where α and β are again (here geometrical) factors which determine the admixture of absorption $\chi''(\omega)$ and dispersion $\chi'(\omega)$. As with other configurations, if $I_cR\sim V$ and here $L\lesssim\delta$, then the ESR signal is roughly $I_c[\alpha\chi'(\omega)+\beta\chi''(\omega)]$ and, for modest N-layer concentration of impurities, it can be an appreciable fraction of I_c (see Sec. IV).

E. ac SQUID geometry

For the measurement of ESR, a considerable improvement in sensitivity, over the point-contact arrangement described above, might be achieved by the use of a double contact or ac SQUID arrangement. This same type of structure can also facilitate the application of a static field as a means of meeting or modifying the resonance condition (3.7). As illustrated in Fig. 3, such a system comprises two junctions in a low inductance loop. In our analysis we assume that the two junctions are point contacts or resistively shunted with negligible capacitance.

In the presence of a magnetic field, the two junctions will no longer oscillate in phase. There will be a circulat-

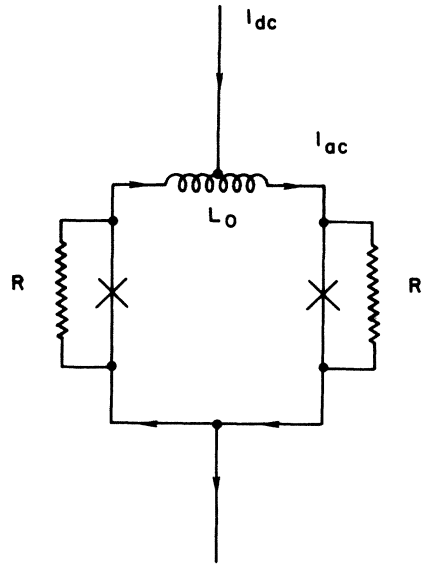

FIG. 3. Schematic of an ac SQUID. The crosses indicate the Josephson junctions. The inductance L_0 is that of the loop, while R is the effective resistance of the junctions including any actual shunt resistances. The sample lies within the inductance coil.

ing current of magnitude $I_c \sin\pi(H/H_Q)$. Here H_Q is the characteristic field corresponding to one quantum of flux penetrating the loop.

The conservation of current gives in complex notation

$$I_c \sin[\pi(H/H_Q)] = [(2\mu_0/i\omega\mu L_0) + 1/R]V \ , \tag{3.30}$$

where μ is the permeability of the magnetic material enclosed in the loop, L_0 its inductance without such a material, and V is the potential difference across each junction. Assuming $\chi(\omega) \ll 1$, in real notation, V is given by

$$V = \{[1/R + (2/\omega L_0)\chi'']^2 + [(2/\omega L_0)(1-\chi')]^2\}^{-1/2} \times I_c \sin[\pi(H/H_Q)]\cos(\omega t + \theta_0) \ , \tag{3.31}$$

where

$$\tan\theta_0 = \frac{2(1-\chi')/\omega L_0}{\frac{1}{R} + (2/\omega L_0)\chi''} \ . \tag{3.32}$$

Following the same steps as for a single point contact, we easily arrive at the following expression for the change in dc current:

$$\Delta I_{dc} = \tfrac{1}{2}(2e/\hbar)(I_c^2/\omega)\sin[\pi(H/H_Q)]\{[1/R + (2/\omega L_0)\chi'']/[1/R + (2/\omega L_0)\chi'']^2 + [(2/\omega L_0)(1-\chi')]^2\} \ . \tag{3.33}$$

Clearly the best coupling to magnetic system is provided when $R \sim \omega L_0$. The magnetic response is of the form

$$(\Delta I_{dc})_{max} \sim \tfrac{1}{2}[(I_c R)^2/VR]\sin\pi(H/H_Q) \times [\alpha\chi'(\omega) + \beta\chi''(\omega)] \ , \tag{3.34}$$

where α and β are of order unity. For much higher frequencies (HF)

$$(\Delta I_{dc})_{HF} \sim [(I_c R)^2/V\omega L_0]\sin[\pi(H/H_Q)]\chi''(\omega) \ , \tag{3.35}$$

which is smaller than (3.34) by a factor of $R/\omega L_0$. For much lower frequencies (LF)

$$(\Delta I_{dc})_{LF} \sim \tfrac{1}{4}(I_c^2 \omega L_0/V)\sin[\pi(H/H_Q)]\chi''(\omega) \ , \tag{3.36}$$

which involves a small factor $\omega L_0/R$.

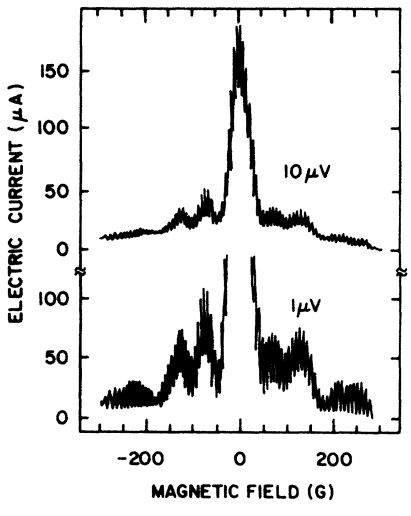

FIG. 4. The electric current as a function of magnetic field for two external potential differences (Ref. 4). The envelope of this "diffraction" pattern is "single-slit"-like and reflects the finite size of the point contacts. The finer oscillations are "two-slit"-like and the period reflects the separation between the, supposed, two-point contacts.

An advantage of this SQUID arrangement as compared with its distributed equivalent, i.e., the thin-film junctions, is the possibility of applying a magnetic field parallel to the loop plane. In this situation the ac field is transverse to the static field, as is required for an ESR experiment, and the applied parallel field can be used to help satisfy the resonance condition. Such an arrangement permits the entire H-ω plane to be investigated. Only the component of **H** parallel to the loop enters the factor $\sin\pi(H/H_Q)$.

To satisfy the above condition $R \sim \omega L_0$ for maximum sensitivity and typical junction impedances, the loop size of the SQUID is limited to micron dimensions. A rough estimate for a loop inductance is $L_0 = \mu_0 R_0 \sim 10^{-6} R_0$ H where R_0 is a dimension of the loop. If a typical ESR resonance frequency is 10 GHz, then a loop of micron dimensions has an impedance $\omega L_0 \sim 10^{-1}$ Ω which is not untypical of Josephson-junction impedances. Physically, such a SQUID might be readily fabricated with the modern microcircuit techniques available at a number of laboratories. A less controlled method is to use rather broad point contacts. Figure 4 shows the magnetic field dependence of the critical current for the point contact for which the measurements on Au:Gd were taken.[5] This exhibits a classic two-contact behavior.

IV. ESTIMATES OF PARAMETERS

The criteria for ESR and finite wave-vector dynamic susceptibility, $\chi(q,\omega)$, measurements differ somewhat and must be treated separately. One common quantity is an estimate of a Curie susceptibility

$$\chi_0 = \frac{(\mu_B g)^2 N_0 S(S+1)}{3kT} \ , \tag{4.1}$$

where N_0 is the number of spins per cubic meter. To estimate χ_0 for a typical system, we take $g = 2$, $S = 3$, and $T = 1$ K and a concentration of sites occupied by magnetic ions of 1000 ppm and obtain

$$\chi_0 \sim 10^{-3} \ .$$

While (4.1) is valid only for dilute paramagnets, the same formula might be used to roughly estimate χ for ordered concentrated magnetic systems near their transition temperatures, i.e., in the hydrodynamic regime. For a transition temperature in the range $\sim 1-10$ K, this gives $\chi \sim 1-0.1$.

For the spin-wave response of ordered systems well below the transition temperatures, results from standard spin-wave theory will be used.

A. Wave-vector-dependent dynamic susceptibility $\chi(q,\omega)$

The usual theory for the ac Josephson effect is valid up to frequencies corresponding to twice the gap or $\sim 3.5kT_c$. The corresponding Josephson frequency is in the range 500—1000 GHz, which would be about 10% of the way to the Brillouin-zone (BZ) edge if the maximum energy of the branch were 300 K $\sim$ 6000 GHz.

The maximum wave vector depends more on junction parameters. For an *SIS* junction the effective *magnetic* thickness of the barrier is $d=2(\lambda+a)\sim 0.1$ μ, while for an *SNS* junction the actual *N*-layer width could be of the order of a micron or more. Finite critical currents have been detected with *N* layers of a few tens of microns. The *N* layer may be either clean or dirty, which results in the critical current and I_cR being different for equal barrier thicknesses. Experiments on dirty *N* layers indicate that thicknesses of a few microns correspond to I_cR products in the 10-μV region. Higher products would result for clean *N* layers. Thus for clean *SNS* junctions one might expect a reasonable (but *not* optimal) $2e(I_cR)\sim\hbar\omega$ with *N* layers of thickness 10 μ. For an *SNS* junction, typically $a \gg \lambda$ and the magnetic and actual barrier thicknesses are practically the same. The one-to-two order-of-magnitude-larger magnetic barrier thickness, as compared with *SIS* junctions, increases the maximum wave vector which can be generated with a given magnetic field by the same factors.

If the superconductor is to be of type I the critical field will be at most several hundred Gauss. However, thin films of thickness less than the coherence length have greatly increased critical fields and, of course, if type-II superconductors were used the upper critical field, create no practical limitation. We take 10^3 G as the upper limit for the experimental field. Equation (2.11b) may be written in the form

$$k_0=\frac{2\pi B_0 d}{\varphi_0} , \tag{4.2}$$

where $\varphi_0=h/2e\sim 2\times 10^{-15}$ Wb is the flux quantum for $d\sim 10^{-5}$ m, and $B_0\sim 0.1$ T, $k_0\sim 3\times 10^9$ m^{-1}. A typical BZ vector q_{BZ} would correspond to an inverse lattice spacing of 2 Å, so

$$q_{\mathrm{BZ}}\sim 0.5\times 10^{10}\ \mathrm{m}^{-1} .$$

Thus, the maximum wave vector that can be probed is greater than 10% of q_{BZ}.

However, the realization of such larger wave vectors implies restrictions upon the junction geometry. For such large frequencies, the theory of Sec. II is inadequate for several reasons but principally because it uses local electrodynamics. Despite this, the theory can be used to give indications about the critical dimensions. The imaginary part of q is determined by $1/\Delta$ and the equivalent of (2.32) when $q\lambda_L>1$ is

$$1/\Delta^2=(\lambda_L^2/\lambda a)K^2 ,$$

with $\mu_S=\mu_M=\mu_0$. From (2.26), when $q\lambda_L>1$, $1/\lambda^2\sim k_n^2$, and if $1/\Delta$ is to be small compared with $k_n\sim q$, then we must have

$$a>\lambda_L(q\lambda_L) ,$$

which with $\lambda_L\sim 10^{-7}$ m, $q\sim 10^9$ m^{-1}, implies that $a>10^{-5}$ m, which is possible for *SNS* junctions. However, for the voltages corresponding to such high frequencies the normal current density would most certainly be too high, leading to heating effects, and because the *N* layer is so thick, the critical current will be too small. To increase the critical current, a value of $d\sim 10^{-5}$ m would be better and an *SNIS* configuration would freeze out the normal current. However, it should still remain possible to probe several percent of the BZ.

Other configurations might be more practical. For example, an *SNISN'* junction might be used. The *SNIS* part would be chosen to maximize the q range, etc. The sample would be the thin *N'* layer. If its thickness is less than the skin depth and the mean free path of the magnons, the magnetic field will only couple to those magnon modes with a zero wave-vector component perpendicular to the plane of the layer. Hence the quantization condition rather than the q vector of the magnetic field would determine this component and the wave vector of the magnons would be well defined.

On the basis of both energy and wave-vector limitations, we estimate that the Josephson-junction $\chi(q,\omega)$ spectroscopy will be useful for measurements up to a few percent of the way toward th BZ edge. This is just the region where neutron measurements become difficult.

The signal observed via the junction I-V curve should be large. We take the following form to crudely represent the magnetic susceptibility associated with dispersive spin waves:

$$\chi(q,\omega)\sim\frac{(\mu_B g)^2 N_0 S(S+1)}{\hbar(\omega_q-\omega+i\Gamma)} . \tag{4.3}$$

The imaginary part of this, at resonance ($\omega=\omega_q$), is

$$\chi''=\frac{(\mu_B g)^2 N_0 S(S+1)}{\hbar\Gamma} . \tag{4.4}$$

If we take rather arbitrarily $\Gamma=1$ K, we obtain

$$\chi''\sim 1 ,$$

indicating an enormous response such that $I_{\mathrm{dc}}\sim I_c$. Such measurements should be easily made.

Clearly these estimates are quite crude. They are intended only to indicate the feasibility of our method and as a guide for the reader who may wish to make estimates for some particular material or junction configuration.

Also of interest is the response of concentrated magnetic systems in the hydrodynamic regime. Then the absorp-

tion is of the form[18]

$$\chi''(q,\omega)=\chi_0\{Dq^2\omega/[\omega^2+(Dq^2)^2]\} . \quad (4.5)$$

This is a slowly varying function of ω width with a maximum value for χ'' of the same magnitude as the static χ_0. Near the maximum and with the susceptibility $\chi_0 \sim 1-10^{-1}$, the response should again be a large fraction of I_c.

B. ESR spectroscopy

Consider specifically the systems Au:Gd^{3+} and Au:^{167}Er. In each case the magnetic ion has a zero-field resonance. For Gd^{3+} this is due to single-ion crystal-field splitting, while for ^{167}Er, the hyperfine coupling is responsible. In both cases the frequency is a few GHz corresponding to voltages of several μV. The resonances are known[19] to be relatively narrow and so, although the static susceptibility for a concentration of 1000 ppm is only $\sim 10^{-3}$, the imaginary part of the dynamic susceptibility is much larger, being $\sim 10^{-1}$ when the resonance condition is satisfied. If the junction parameters are chosen so that $I_cR \sim V$ (where 2 eV/$\hbar=\omega_s$ and ω_s is the frequency for resonance), then from Eq. (3.28) the response is

$$I_{dc} \sim I_c[\alpha\chi'(\omega)+\beta\chi''(\omega)] \sim 10^{-1}I_c ,$$

which is again large.

These estimates are confirmed by the measurements of Baberschke *et al.*[5] In Fig. 5 we reproduce the I-V curve for a point-contact *SNS* device in which the N layer was Au:1000 ppm Gd. The indicated ESR response is indeed an appreciable fraction of I_c. Figure 6 shows data for a much less concentrated 100-ppm sample. A comparison with the state-of-the-art measurements with a conventional ESR spectrometer[20] shows at least an order of magnitude improvement in the signal-to-noise ratio. These preliminary measurements, therefore, indicate that concentrations of a couple of orders of magnitude smaller might be detected with the Josephson technique.

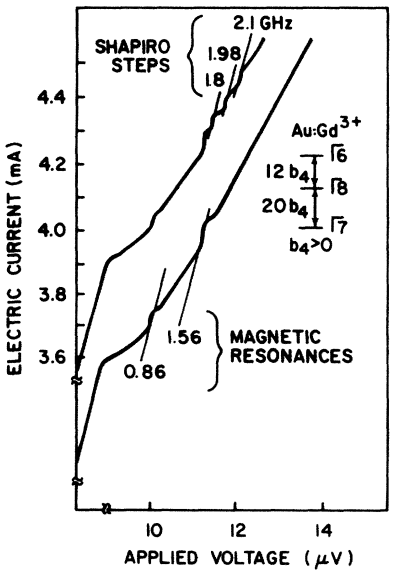

FIG. 5. I-V curves for a Nb-Au—1000-ppm Gd-Nb *SNS* Josephson junction (Ref. 5). The lower curve shows two magnetic resonance features corresponding to the transitions between the crystal-field split levels shown on the right. The upper curve shows Shapiro steps used to calibrate the frequency.

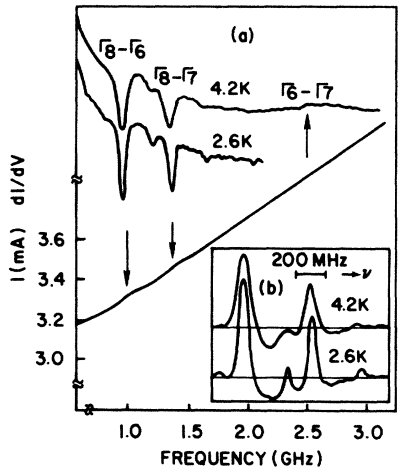

FIG. 6. Actual I-V and dI/dV curves for an Au:100-ppm Gd experiment (Ref. 5). The inset shows the dI/dV curve, inverted, with the smooth nonresonance part of the curve subtracted. This latter curve shows at least an order of magnitude improvement in intensity over the conventional ESR for this system (Ref. 20). Different temperatures were measured to show that paramagnetic (Korringa) relaxation was occurring.

V. CONCLUSIONS AND DISCUSSION

We have developed a theory for wave-vector-dependent dynamic susceptibility and ESR measurements for a variety of Josephson-junction geometries. These include *SIS*, *SNS*, *SISN*, and *SINS* planar junctions. In addition, the theory for the point-contact *SNS* junctions and SQUID arrangements relevant to recent experiments has been described. Estimates of the various parameters have been given.

Measurements by Baberschke *et al.*[5] have confirmed our estimates for ESR in point-contact *SNS* structures developed by Pellisson *et al.*[3] and show the technique to be practical. It is easy to argue that under favorable circumstances the currently proposed technique represents the ultimate radio spectroscopic ESR or $\chi(q,\omega)$ measurement for a metallic sample. Consider the excess current $I_e=I-(I/R)$, i.e., the difference between the actual current and what the current would be if the junction were purely resistive. Since I_eV represents a power supplied to the junction, it must be that the excess current is associated with some loss mechanism. It is not difficult to identify this loss as being due to the normal current in the N layer at the frequency observation ω. To this we add the observation that this current is restricted to the region of the junction which is occupied by the magnetic system under observation and for this reason it is intrinsic to the measurement. We then compare this to a standard ESR experiment. In such an experiment there is the identical loss mechanism in the region of the sample which is

observed due to the absorption of power by the currents which screen the applied rf field. Clearly, in both cases there is a noise associated with these normal currents which is intrinsic to the experiment and unavoidable. Under the circumstances envisaged in this paper, $I_e \sim I$ and so the noise associated with I and I_e are comparable, while in practice these two are the principal noise source intrinsic to the device. Finally, with a high quality SQUID it is realistic to expect that the noise associated with the I-V measurement is no greater than that generated by the measuring device. We conclude that the envisaged spectroscopic measurement is limited only by the unavoidable rf noise generated by the sample adding another Josephson-type measurement to those which are limited only by intrinsic considerations.

Dynamic susceptibility, $\chi(q,\omega)$ measurements for wave vectors q up to several percent of the way to the BZ edge appear to be possible. The estimated response is so large that potentially less sensitive, but more convenient, *SISN* geometries might be used. The normal sample forming the N layer might be evaporated on prefabricated *SIS* junctions. The response is less because, except for very thin films of thickness less than the London penetration depth, the rf field, and therefore the coupling of the Josephson effect to the magnetic system, decays exponentially with the S-layer thickness.

The principal difficulties of this technique for spectroscopic measurements are the need to make the sample a part of the junction, the restriction to the low temperatures necessary for superconductivity, and the problem that type-I superconductivity will only coexist with low magnetic fields.

Possible solutions to these problems consist of the use of point contacts developed by Pellisson *et al.*[3] and used in the measurements by Baberschke and co-workers,[4,5] in which case the sample consisted of a rolled foil of Au:Gd. Another possibility which would permit the use of bulk samples in both $\chi(q,\omega)$ and ESR measurements is again the use of pre-evaporated *SNS* or *SIS* junctions simply placed in close physical contact with a bulk sample. Since the important coupling is inductive, good electrical contact is not essential. This has been confirmed by studies of *NISISIN* structures not reported here. For junctions with a large resistance, lumped SQUID geometries, which physically separate the sample and Josephson device, might be possible. Larger fields necessary to perform some ESR measurements could be facilitated if the magnetic field were generated by control lines well separated from screened junctions. Devices might also be fabricated from type-II superconductors. One might even envisage, within the bounds of existing microelectronic technology, the local heating of the sample by resistive control lines.

Interesting possibilities for this technique are numerous. In particular, the possibility of measuring $\chi(q,\omega)$ for very low wave vectors would permit the study of critical dynamics for the hydrodynamic regime of concentrated magnets. Perhaps more exciting is the possibility of similar studies on spin-glasses. Such studies might well confirm or reject the possibility of the existence of a spin-glass phase transition. The small size and low power requirements of Josephson-junction spectroscopy are compatible with the use of dilution refrigerators to attain very low temperatures. ESR measurements on very dilute "ideal" spin-glasses at temperatures less than 1 K would be possible. The dynamics of single-ion (or possibly lattice) Kondo systems might also be studied at low temperatures.

There is also the speculative but interesting possibility that *SN* point contacts might be used for ESR and perhaps $\chi(q,\omega)$ measurements. The existence of an ac Josephson effect seems to have been demonstrated for point contacts of this kind.[21] In fact, the "series" resistance needed in the analysis of the recent ESR work with *SNS* point contacts[5] suggests that either the top or the bottom *SN* contact was not good and that these were, in effect, *SN* point-contact measurements. It is hoped to develop a detailed theory for this possibility in the near future.

Finally, it is interesting to note that there is an appreciable coupling of the ac Josephson effect to phonon modes in *SIS* junctions.[22] A rather straightforward extension of the present theory to include lattice currents might explain the current data. Should such an approach prove correct, it would appear that the Josephson effect is capable of producing not only monochromatic photons but also phonons with a well-defined wave vector. There are no skin-depth problems associated with phonons and again if our estimates are accurate it will be possible to extend this technique,[22] currently only selective with respect to the frequency, to one which would measure *phonon* dispersion relations up to a few percent of the way into the BZ.

[1]A. H. Silver and J. E. Zimmerman, Appl. Phys. Lett. **10**, 142 (1967).

[2]S. E. Barnes, J. Phys. C **10**, 2863 (1977).

[3]J. Pellisson, R. Delescelfs, and S. E. Barnes (unpublished).

[4]K. D. Bures, K. Baberschke, and S. E. Barnes, in *Proceedings of the 17th International Conference on Low Temperature Physics,* edited by U. Eckern, A. Schmid, W. Weber, and H. Wühl (North-Holland, Amsterdam, 1984), p. 827.

[5]K. Baberschke, K. D. Bures, and S. E. Barnes, Phys. Rev. Lett. **53**, 98 (1984).

[6]A. M. Goldman, C. G. Kuper, and O. T. Valls, Phys. Rev. Lett. **52**, 1440 (1984).

[7]R. E. Eck, D. J. Scalapino, and B. N. Taylor, Phys. Rev. Lett. **13**, 15 (1964).

[8]R. E. Eck, D. J. Scalapino, and B. N. Taylor, in *Proceedings of the 9th International Conference on Low Temperature Physics,* edited by J. G. Daunt (Plenum, New York, 1965), p. 415; I. O. Kulik, Zh. Tekhn. Fiz. **37**, 157 (1967) [Sov. Phys.—Tech. Phys. **12**, 111 (1967)]; W. Liniger and F. Odeh, J. Franklin Inst. **307**, 245 (1979).

[9]M. D. Fiske, Rev. Mod. Phys. **36**, 221 (1963); D. D. Coon and M. D. Fiske, Phys. Rev. **138**, A744 (1965).

[10]S. E. Barnes, J. Appl. Phys. **51**, 6438 (1980).

[11]K. Bures, S. E. Barnes, and K. Baberschke, J. Appl. Phys. **54**, 7073 (1983).

[12]F. London and H. London, Proc. R. Soc. London, Ser. A **149**,

72 (1935).
[13]B. D. Josephson, Phys. Lett. **1**, 251 (1962); Rev. Mod. Phys. **36**, 216 (1964); Adv. Phys. **14**, 419 (1965); D. N. Langenberg, D. J. Scalapino, and B. N. Taylor, Proc, IEEE **54**, 560 (1966).
[14]A. B. Pippard, Proc. R. Soc. London, Ser. A **191**, 399 (1947); J. C. Swihart, J. Appl. Phys. **32**, 461 (1961).
[15]See, for example, A Abragam, *The Principles of Nuclear Magnetism* (Clarendon, Oxford, 1961), p. 40.
[16]J. Korringa, Physica **16**, 601 (1950).
[17]See, for example, A Barone and G. Paterno, *Physics and Applications of the Josephson Effect* (Wiley-Interscience, New York, 1982), p. 121.
[18]H. A. Bennett and P. C. Martin, Phys. Rev. **138**, A608 (1965); B. I. Halperin and P. C. Hohenberg, Phys. Rev. **188**, 898 (1969).
[19]S. E. Barnes, Adv. Phys. **30**, 801 (1981).
[20]E. P. Chock, R. Chui, D. Davidov, R. Orbach, D. Shaltiel, and L. J. Tao, Phys. Rev. Lett. **27**, 582 (1971); K. Baberschke and Y.v. Spalden, Phys. Rev. B **19**, 5933 (1979).
[21]G. Voss, Ph.D. thesis, University of Köln, 1984.
[22]H. Kinder, P. Berberich, and A. Schick, Physica **126B**, 193 (1984), and references therein.

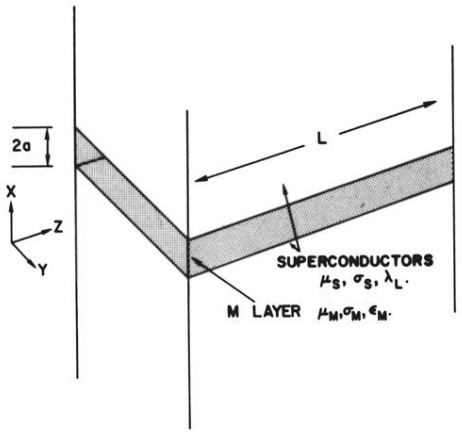

FIG. 1. Geometry of the *SMS* Josephson junction, where *S* denotes a superconductor and *M*, the middle layer, is either an insulator or a normal metal. Either the *S* or the *M* layer may contain the magnetic system.